# Topologically invariant tensor renormalization group method for the Edwards-Anderson spin glasses model

Chuang Wang,[1,2,*] Shao-Meng Qin,[1] and Hai-Jun Zhou[1]
[1]*State Key Laboratory of Statistical Physics, Institute of Theoretical Physics, Chinese Academy of Sciences, Zhong-Guan-Cun East Road 55, Beijing 100190, China*
[2]*University of Chinese Academy of Sciences, Beijing 100049, China*
(Received 26 November 2013; revised manuscript received 23 October 2014; published 10 November 2014)

Tensor renormalization group (TRG) method is a real space renormalization group approach. It has been successfully applied to both classical and quantum systems. In this paper, we study a disordered and frustrated system, the two-dimensional Edwards-Anderson model, by a new topological invariant TRG scheme. We propose an approach to calculate the local magnetizations and nearest pair correlations simultaneously. The Nishimori multicritical point predicted by the topological invariant TRG agrees well with the recent Monte Carlo results. The TRG schemes outperform the mean-field methods on the calculation of the partition function. We notice that it might obtain a negative partition function at sufficiently low temperatures. However, the negative contribution can be neglected if the system is large enough. This topological invariant TRG can also be used to study three-dimensional spin glass systems.

DOI: 10.1103/PhysRevB.90.174201 PACS number(s): 75.10.Nr, 05.10.Cc, 64.60.De

## I. INTRODUCTION

Exploring the Edwards-Anderson (EA) model [1] is significant but extremely difficult. The nature of spin glasses in three dimensions—between the mean-field picture and droplet picture [2–7]—has been much debated over the past 30 y. The two-dimensional (2D) model, besides attractiveness in statistical physics, has wild applications on image processing [8] and computer vision [9,10], which is usually referred to as the Markov random field [11] in the computer science community. In this paper, we propose a coarse-graining method for the EA model on a 2D square lattice and calculate local physical quantities simultaneously by the tensor renormalization group (TRG) method.

TRG is a real space renormalization group approach initially introduced by Levin and Nave [12] for classical ferromagnetic Ising spin systems on 2D regular lattices. This method is an extension of the density matrix renormalization group method for 1D quantum systems [13]. The basic idea is to perform a coarse-graining process on a tensor network. Matrix low rank approximation is used to cut the degree of freedom of tensor indices to a maximum value $D$ through the singular value decomposition.

Shortly after the introduction of the initial TRG method, an improvement was made by Xie and coauthors [14], who proposed a backward iteration to calculate the environment tensor and improved the results by considering the effect of the environment. The TRG method has excellent performance on the classical ferromagnetic Ising model, the Potts model [15], the diluted ferromagnetic model [16,17], etc. It also becomes a crucial tool to handle 2D quantum systems [18–20]. Very recently a further improvement, namely the topological invariant TRG method, was proposed in the papers [21,22] to extend the TRG to 3D ferromagnetic Ising cases.

Unlike the ferromagnetic Ising model, the EA spin glass model [1] is heterogeneous, disordered, and frustrated. It is intrinsically hard. The problems of finding a ground state of the 2D EA model with external field and the general 3D EA model are proved to belong to non-deterministic-polynomial-hard (NP-hard) class [23]; it is commonly believed that no algorithm can solve them within polynomial time. In the previous study, the mean-field approximation [24–28] and Monte Carlo sampling [29], transfer matrix method [30], and numerical exact algorithm for 2D without the external field [23,31] are used to calculate local properties for individual finite size instances. These methods are combined with finite size scaling to investigate the thermodynamic limit properties. The duality relationship [32–34] and real space renormalization methods [35] are also employed to study the phase diagram and universality. TRG can be exploited in both of two roles. It can be served as an approximate calculator of physics quantities for a single instance, and it may also be used as a new renormalization method to directly investigate critical phenomenon. We here focus on the former role.

In this paper, we propose two main approaches. First, we show a new topological invariant coarse-graining scheme based on the work [21]. It avoids two problems when the method [21] is directly applied on EA model: cutting extra freedom of indices and inversing singular matrices. In the ferromagnetic Ising model, these two problems do not exist. Second, we propose an approach to compute local physical quantities simultaneously. For example, all single-spin magnetizations can be calculated by a single sweep of coarse-graining procedure and backward procedure. These two approaches are also useful for other heterogeneous systems. In the numerical calculation, TRG may get a negative value of the partition function at very low temperature, which is the major difference between the spin glass model and other heterogeneous systems [16,17]. We show that the contribution of the negative part is comparable to the error fluctuation for a large enough system and, therefore, it can be neglected. In the high-temperature region, TRG outperforms the mean-field method, belief propagation, and generalized belief propagation [24–28], while the mean-field methods are failed in the

*wangchuang@itp.ac.cn

 

lower temperature because of the convergence problems. The Nishimori multicritical point [32,36,37] is calculated by our TRG scheme. The results agree well with the recent Monte Carlo results [29]. We emphasize that the original TRG method [12] can also be directly applied to any heterogeneous systems, including the EA model, similar to the works on the diluted ferromagnetic model [16,17]. The advantage of topological invariant scheme is that it can be extended to 3D cases [21,22].

The paper is arranged as follows. In the remainder of this section, we introduce the EA model and show how to convert it to a tensor network. In Sec. II, we demonstrate our topological invariant TRG procedure. In Sec. III, we show how to calculate local physical quantities by backward iteration. In Sec. IV, we list some numerical results to test the validation of this method. In Sec. V, we discuss further improvement and applications.

## II. THE MODELS

### A. The Edward-Anderson model

We consider the classical 2D EA model on a periodic square lattice with discrete coupling constants. The system consists of $N$ spins $\{\sigma_i\}$, $M$ coupling constants $\{J_{ij}\}$, and $N$ local external fields $\{h_i\}$. Each spin $\sigma_i$ takes value from $\{+1,-1\}$. The overall spin state $\underline{\sigma} = (\sigma_1,\sigma_2,\ldots,\sigma_N)$ is referred to as a configuration. The energy function is defined as

$$H(\underline{\sigma}) = -\sum_{(ij)\in E} J_{ij}\sigma_i\sigma_j - \sum_{i\in V} h_i\sigma_i, \tag{1}$$

where $E$ and $V$ denote the edge set and vertex set of the system, respectively.

For a single instance of the EA model, the coupling constants and local external fields are fixed according to predefined distributions. In this paper, the value of $J_{ij}$ is randomly chosen from the binomial distribution $P(J_{ij}) = p\delta(J_{ij},1) + (1-p)\delta(J_{ij},-1)$, where $\delta(x,y)$ is the Kronecker $\delta$ symbol, which is 1 if $x = y$; otherwise it is 0. The model parameter $0.5 \leqslant p \leqslant 1$ alters the system ranging from the spin glass ($p = 0.5$) to the pure ferromagnetic system ($p = 1$). The configuration $\underline{\sigma}$ is supposed to follow the Gibbs-Boltzmann distribution,

$$p(\underline{\sigma}) = \frac{1}{Z}\exp[-\beta H(\underline{\sigma})],$$

where $Z = \sum_{\underline{\sigma}} \exp[-\beta H(\underline{\sigma})]$ is the partition function. It is useful to rewrite the distribution as a production of a set of non-negative weight factors,

$$p(\underline{\sigma}) = \frac{1}{Z}\prod_{(ij)\in E}\psi_{ij}(\sigma_i,\sigma_j)\prod_{i\in V}\psi_i(\sigma_i), \tag{2}$$

where the weight factors have the form $\psi_{ij}(\sigma_i,\sigma_j) = \exp[\beta J_{ij}\sigma_i\sigma_j]$, $\psi_i(\sigma_i) = \exp[\beta h_i\sigma_i]$. If all the external random fields are zero, the partition function and the pair-spin correlations can be calculated exactly in polynomial time [23,31,38]. However, for general external fields $\{h_i\}$, the problem is proved to be in the NP-hard class [23].

### B. Tensor networks

Any two-body interaction system can be transformed into a tensor network, in which the partition function of the system is equal to the trace of all the tensors. The transformation is not unique. Here we show a symmetric method. The transformation of the EA model on 2D square lattice at a site $i$ is illustrated in Fig. 1. First each Ising spin $\sigma_i$ is mapped to a Boolean variable $s_i = (1-\sigma_i)/2 \in \{0,1\}$, so that each weight factor $\psi_{ij}(\sigma_i,\sigma_j)$ can be expressed as a matrix $\Phi^{(ij)}$, where the element in $s_i$th row and $s_j$th column is $\Phi^{(ij)}_{s_i s_j} = \psi_{ij}(1-2s_i,1-2s_j)$. Note that the C-programming-language convention is used, in which the index starts from 0. Meanwhile, each external weight factor $\psi_i(\sigma_i)$ of field $h_i$ is mapped to a vector $\Phi^{(i)}$, of which the $s_i$th element is $\Phi^{(i)}_{s_i} = \psi_i(1-2s_i)$. Next we perform the singular value decomposition on the matrix $\Phi^{(ij)}$, such that

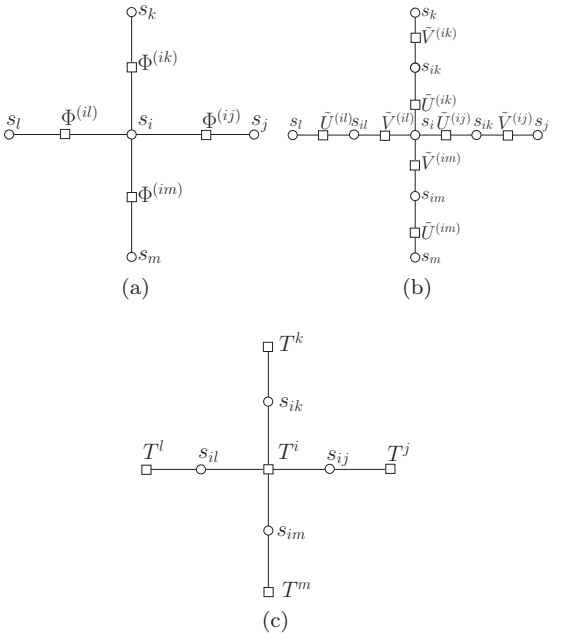


FIG. 1. Construction of a tensor network. (a) The neighborhood of a vertex $i$. (b) Each matrix $\Phi^{(ij)}$ is split into two matrices by the singular value decomposition, so that each vertex $i$ is now surrounded by four matrices which share the common index $s_i$. (c) Summing over the index $s_i$, the four neighboring matrices contract to be a tensor $T^i$.

$$\Phi^{(ij)}_{s_i s_j} = \sum_{s_{ij}} U^{(ij)}_{s_i s_{ij}} d_{s_{ij}} V^{(ij)}_{s_j s_{ij}}, \tag{3}$$

where the matrices $U^{(ij)}$, $V^{(ij)}$ are real orthogonal matrices and the vector $\underline{d} = (d_0,d_1)$ stores singular values in descending order. Each element in the vector $\underline{d}$ is non-negative. The new variable $s_{ij} \in \{0,1\}$ is the index of the singular vector $\underline{d}$. Let $\tilde{U}^{(ij)}_{s_i s_{ij}} = U^{(ij)}_{s_i s_{ij}} d^{\frac{1}{2}}_{s_{ij}}$, $\tilde{V}^{(ij)}_{s_j s_{ij}} = V^{(ij)}_{s_j s_{ij}} d^{\frac{1}{2}}_{s_{ij}}$. Then we have

$$\Phi^{(ij)}_{s_i s_j} = \sum_{s_{ij}} \tilde{U}^{(ij)}_{s_i s_{ij}} \tilde{V}^{(ij)}_{s_j s_{ij}}.$$

Now, each variable $i$ is surrounded by four matrices, $\tilde{U}^{(ij)}_{s_i s_{ij}}$, $\tilde{U}^{(ik)}_{s_i s_{ik}}$, $\tilde{V}^{(il)}_{s_i s_{il}}$, $\tilde{V}^{(i,m)}_{s_i s_{im}}$, where $j,k,l,m$ are labels of the neighbor spins of spin $i$. Finally, we sum over $s_i$ and get a tensor

$T^i_{s_{ij}s_{ik}s_{il}s_{im}}$:

$$T^i_{s_{ij}s_{ik}s_{il}s_{im}} = \sum_{s_i} \tilde{U}^{(ij)}_{s_i s_{ij}} \tilde{U}^{(ik)}_{s_i s_{ik}} \tilde{V}^{(il)}_{s_i s_{il}} \tilde{V}^{(i,m)}_{s_i s_{im}} \Phi^{(i)}_{s_i}. \quad (4)$$

The partition function of the original system is equal to the result obtained by tracing over all the indices of the tensors defined on lattice sites:

$$Z = \sum_{\{s\}} \prod_i T^i_{s_{ij}s_{ik}s_{il}s_{im}}. \quad (5)$$

We refer to the network of tensors constructed by the above procedure as a tensor network. On the original lattice, each vertex $i$ is associated with a tensor $T^i$, and each edge $(ij)$ is associated with a tensor index $s_{ij}$. In graphical language, the tensor network is similar to a factor graph model with weight factors defined on vertices and state variables defined on edges, but a key difference is that the elements of tensors are not necessarily non-negative. In the following discussions, we rewrite the tensor indices as $i_0,i_1,i_2,i_3$, i.e., $T^i_{i_0 i_1 i_2 i_3}$ for notational simplicity.

## III. TENSOR COARSE-GRAINING PROCEDURE

There are several ways to implement the tensor coarse-graining procedure [12,21,22]. Generally, each coarse-graining iteration consists of two steps. First is contracting two neighbor tensors into a new tensor with bigger degrees-of-freedom indices. It is an exact procedure. If there is no computation limitation, the exact partition function could be gotten by the iteration of these contractions. Second is cutting the degrees-of-freedom indices approximately, so that the computation is tractable.

We introduce our method for the tensor network defined on a 2D square lattice with the periodic boundary condition expressed as Eq. (5). At the first step, each two vertical neighbor-tensor pairs $T, T'$ are contracted as shown in Fig. 2(a). We sum over the common index $k$, and the pair $T,T'$ is unified into one tensor $R$:

$$R_{(i_0,j_0),j_1,(i_2,j_2),i_3} = \sum_k T_{i_0,k,i_2,i_3} T'_{j_0,j_1,j_2,k}. \quad (6)$$

The new tensor $R$ has six indices $i_0$, $i_2$, $i_3$, $j_0$, $j_1$, $j_2$. We combine two indices in the same direction $i_0$, $j_0$ as a union index $\hat{i}_0$ and $i_2$, $j_2$ as another union index $\hat{i}_2$, so that the number of indices of $R$ is still four, i.e., $\hat{i}_0$, $j_1$, $\hat{i}_2$, $i_3$. After the contraction, the topological structure of the square lattice is preserved, and the $y$ direction length shrinks to half, while the degrees-of- freedoms indices associated with the edges along the $x$ direction increases to the square of the previous one.

At the second step, the union indices $\hat{i}_0$ and $\hat{i}_2$ will be truncated alternatively along the $x$ direction if their degrees of freedom are greater then a given cutoff parameter $D$. Specifically, let us consider the two horizontal neighbor tensors $R_{\hat{k},j_1,\hat{i}_2,i_3}$ and $R'_{\hat{i}'_0,j'_1,\hat{k},i'_3}$ in Fig. 2(b), which share an index $\hat{k}$. We think of $R$ and $R'$ as a subsystem in the tensor network with the internal variable $\hat{k}$ and the boundary variables $\{j_1,\hat{i}_2,i_3\}$ and $\{\hat{i}'_0,j'_1,i'_3\}$. The boundary variables interact with other tensors, which can be considered as the environment of the subsystem. We are going to approximate the subsystem with another one with a lower degree of freedom of internal variable such that the interaction with environment is as similar as possible. Mathematically, it is done by the lower rank matrix approximation. We rearrange the indices order of the tensor $R$ as $j_1,\hat{i}_2,i_3,\hat{k}$ and group the first three indices as an unique index $\underline{i} = (j_1,\hat{i}_2,i_3)$. Then tensor $R$ becomes a matrix $R_{\underline{i},\hat{k}}$. In the same way, we get the matrix $R'_{\hat{k},\underline{i}'}$ from the tensor $R'$, where $\underline{i}' = (\hat{i}'_0,j'_1,i'_3)$. We sum over the common index $\hat{k}$ to get a new matrix $A$:

$$A_{\underline{i},\underline{i}'} = \sum_{\hat{k}} R_{\underline{i},\hat{k}} R'_{\hat{k},\underline{i}'}. \quad (7)$$

The subsystem is now expressed by the matrix $A$. To exactly represent the boundary interaction, the minimum degree of freedom of the internal variable is of rank $A$. A lower rank approximation is made by the singular value decomposition. The matrix $A$ is decomposed in the reduced form by

$$A_{\underline{i},\underline{i}'} = \sum_{k'=0}^{\mathrm{rank}(A)-1} U_{\underline{i},k'} d_{k'} V_{\underline{i}',k'}. \quad (8)$$

The reduced singular value decomposition discards the zero elements of the singular vector $d$, which has no contribution to the subsystem. In the numerical computation, singular values less than the criterion $d_i < \epsilon = 10^{-12}$ are considered to be zero. If the rank of $A$ is greater than the cutoff parameter $D$, we only keep the largest $D$ singular values. Let $a' = \min\{\mathrm{rank}(A), D\}$. The approximation of $A$ is expressed as

$$A_{\underline{i},\underline{i}'} \approx \tilde{A}_{\underline{i},\underline{i}'} = \sum_{k'=0}^{a'-1} \tilde{T}_{\underline{i},k'} \tilde{T}'_{\underline{i}',k'}, \quad (9)$$

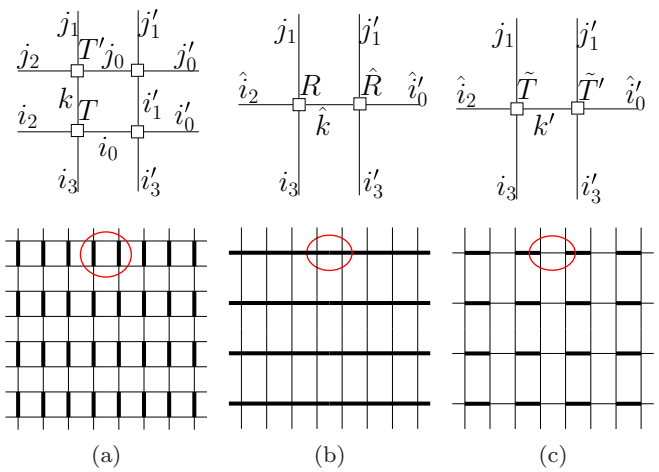


FIG. 2. (Color online) Demonstration of TRG. The top figure is the microscope of the circled region in the bottom figure. The two vertical tensors $T$ and $T'$ in (a) are contracted into one tensor $R$ in (b), and the associated two indices $i_0$ and $j_0$ of (a) are combined into one index $\hat{i}_0$. If the degree of freedom of the index $\hat{i}_0$ is larger than the cutoff parameter $D$, we use the singular value decomposition to truncate this index and obtain the approximate tensors $\tilde{T}$ and $\tilde{T}'$ in (c). Bold lines indicate that the freedom of associated indices is greater than the others when the freedom exceeds the cutoff parameter $D$.

where $\tilde{T}_{\underline{i},k'} = U_{\underline{i}',k'} d_{k'}^{\frac{1}{2}}$ and $\tilde{T}'_{\underline{i}',k'} = V_{\underline{i}',k'} d_{k}^{\frac{1}{2}}$. The matrices $\tilde{T}$ and $\tilde{T}'$ are nonsingular, and therefore their inverse matrices always exists. This property will be used in the next section. Next, we expand the grouped indices $\underline{i}$ and $\underline{i}'$ and rearrange the order of indices to recover the tensor $\tilde{T}_{\hat{k},j_1,\hat{i}_2,i_3}$ and $\tilde{T}'_{\hat{i}'_0,j'_1,\hat{k},i'_3}$.

In this way, the tensors $R$ and $R'$ in Fig. 2(b) are replaced by $\tilde{T}$ and $\tilde{T}'$ in Fig. 2(c), and the common index $\hat{k}$ is replaced with $k'$, whose degree of freedom is no greater than $D$. The above procedure of cutting off variable $\hat{k}$ by the singular value decomposition guarantees that the matrix $\tilde{A}$ is a best approximation of $A$ among all matrices with a rank no greater than $D$, if the measure of the error is the Frobenius norm $\|A - \tilde{A}\|_F$. Note that $A$ is a $D^6 \times D^6$ matrix. The complexity of directly decomposition of $A$ is $O(D^{18})$. Considering that the rank of $A$ is at most $D^2$, we could reduce the complexity into $O(D^8)$. Details are illustrated in the Appendix.

We now rotate the present tensor network 90° in Fig. 2(c), and then it has the same local structure of the tensor network as the one at the first step in Fig. 2(a), while the length along the $x$ direction is reduced by half. We repeat steps 1 and 2 once more. The size of the tensor network shrinks by half in both the $x$ and the $y$ directions.

This is the complete step of a coarse-graining procedure. We repeat it until the tensor network is reduced enough to be tractable by brute-force summation to get the partition function. In this paper, the final size is $2 \times 2$.

In practice, the value of elements of the tensors increase exponentially during the TRG procedure. So we need to scale the tensor after each step. The scaling is forcing the maximum singular value of each $\tilde{A}^{(i)}$ in Eq. (9) in the present layer of the tensor network to be a fixed value $S_m$, and we save the logarithm of the scale factor for the $i$th matrix at the $l$th step as

$$\phi_l^{(i)} = \ln\left(d_0^{(i)}\right) - \ln(S_m), \tag{10}$$

where $d_0^{(i)}$ is the maximum singular value of matrix $\tilde{A}^{(i)}$. The total free energy density is

$$f(\beta) = -\frac{1}{N\beta}\left(\sum_l \sum_i \phi_l^{(i)} + \ln Z_r\right), \tag{11}$$

where $Z_r$ is the remaining scaled partition function calculated by contracting the final $2 \times 2$ tensor network.

The cutoff parameter $D$ controls the space of approximate tensors when performing the coarse-graining procedure. If $D$ is infinitely large, the coarse-graining process is exact. Generally, larger $D$ will get more accurate results. In terms of computational complexity, our topological invariant TRG scheme is of order $O(D^8)$, while the original method [12] and the higher order TRG [21] are $O(D^6)$ and $O(D^7)$, respectively. Practically, the precision in calculating the free energy is better than the original one [12] for the same cutoff parameter $D$. Our tensor coarse-graining method is based on the higher order TRG [21], where the exact contraction step is the same, but the approximate truncation is different. The higher order TRG method truncates all the indices associated with $x$-direction edges by the higher order singular value decomposition. However, we found that such a truncation scheme cannot report a sufficiently precise free energy density value for the EA spin glass model. We only truncate the $x$-direction indices alternatively, while the remaining half of the $x$-direction indices will be contracted in the next step, so they are not necessary to be truncated.

## IV. MARGINAL PROBABILITY AND BACKWARD PROCEDURE

The EA model has no translational symmetry, and therefore the local magnetization depends on vertex position. The marginal probability distribution of a vertex $i$ is given by

$$P_i(s_i) = \frac{1}{Z} \sum_{\text{all indices}} T^i(s_i) \prod_{j \in V \setminus \{i\}} T^j, \tag{12}$$

where $s_i$ is related to the spin $\sigma_i$ by $\sigma_i = 1 - 2s_i$ and the term "all indices" under the summation represents all the indices of every tensor in the tensor network $\{T^i | i \in V\}$, and $T^i(s_i)$ is a tensor at vertex $i$ when its spin $\sigma_i$ is fixed to $1 - 2s_i$:

$$T^i_{i_0 i_1 i_2 i_3}(s_i) = \tilde{U}_{s_i i_0} \tilde{U}'_{s_i i_2} \tilde{V}_{s_i i_3} \tilde{V}'_{s_i i_1} \Phi^{(i)}_{s_i}. \tag{13}$$

As shown in Eq. (12), $P_i(s_i)$ can be computed by ordinary TRG method for any $i$ in the tensor network with a special tensor $T^i(s_i)$. However, it is impractical to calculate the marginal probabilities for all the vertices in this way. In this work we use the backward iteration method [14] to compute the marginal spin probability distribution functions for all the vertices simultaneously.

We define the environment tensor, which we simply call the environment, of a local tensor $T^i$ as

$$M^i_{i_0 i_1 i_2 i_3} = \sum_{\substack{\text{all indices} \\ \text{except } i_0,i_1,i_2,i_3}} \prod_{j \in V \setminus i} T^j, \tag{14}$$

where the summation is taken over all the indices of the tensor network except the indices of the tensor $T^i$. An environment $M^i$ has the same indices as its correspondent tensor $T^i$. The partition function can be rewritten as

$$Z = \sum_{i_0 i_1 i_2 i_3} T^i_{i_0 i_1 i_2 i_3} M^i_{i_0 i_1 i_2 i_3}. \tag{15}$$

The marginal probability distribution is expressed as

$$P_i(s_i) = \frac{1}{Z} \sum_{i_0 i_1 i_2 i_3} T^i_{i_0 i_1 i_2 i_3}(s_i) M^i_{i_0 i_1 i_2 i_3}. \tag{16}$$

Similarly, the nearest-neighbor pairwise marginal distribution $P_{ij}(s_i, s_j)$ can be also expressed as a summation between a pair of neighbor tensors and the corresponding environment,

$$P_{ij}(s_i, s_j) = \frac{1}{Z} \sum_{i_0 j_0 j_1 i_2 j_2 i_3 k} T^i_{i_0,k,i_2,i_3}(s_i) T^j_{j_0,j_1,j_2,k}(s_j) \times \hat{M}^{ij}_{(i_0,j_0),j_1,(i_2,j_2),i_3}, \tag{17}$$

where $\hat{M}^{ij}_{(i_0,j_0),j_1,(i_2,j_2),i_3}$ is the environment of the tensor $R_{(i_0,j_0),j_1,(i_2,j_2),i_3} = \sum_k T^i_{i_0,k,i_2,i_3} T^j_{j_0,j_1,j_2,k}$.

We calculate environments of a tensor network at a more detailed level based on knowing the environments at a coarse-grained level, which we called the backward iteration. We start from the final coarse-grained $2 \times 2$ tensor network after

finishing the forward TRG procedure. The corresponding environment $M^i$ of a tensor $T^i$ at this level can be calculated directly by tracing the other three tensors.

Given the environments $M^{\tilde{T}}$, $M^{\tilde{T}'}$ of the tensors $\tilde{T}$, $\tilde{T}'$ in Fig. 2(c), we now show how to calculate the environments $M^T$, $M^{T'}$ of the tensors $T$, $T'$ at the detailed level in Fig. 2(a) . The definition of indices is the same as described in the previous section and shown in Fig. 2. We start from the relation equation of the tensor $\tilde{T}$ and its environment $M^{\tilde{T}}$ in Eq. (15),

$$Z = \sum_{k',j_1,\hat{i}_2,i_3} \tilde{T}_{k',j_1,\hat{i}_2,i_3} M_{k',j_1,\hat{i}_2,i_3} \tag{18}$$

$$= \sum_{k',k'',\underline{i}} \tilde{T}_{k',\underline{i}} \delta^{k'}_{k''} M_{k'',\underline{i}}, \tag{19}$$

where in the second line we group the indices $(j_1,\hat{i}_2,i_3)$ as $\underline{i}$ and insert a Kronecker $\delta$ function $\delta^{k'}_{k''}$.

The tensor $\tilde{T}'_{\hat{i}'_0,j'_1,k',i'_3}$ can be viewed as a matrix $\tilde{T}'_{k',\underline{i}'}$ if we exchange the order of indices to $k',\hat{i}'_0,j'_1,i'_3$ and group the indices $\hat{i}'_0,j'_1,i'_3$ as $\underline{i}'$. As mentioned in previous section, the matrix $\tilde{T}'_{k',\underline{i}'}$ is always nonsingular, and we replace the Kronecker $\delta$ function in Eq. (19) with

$$\delta^{k'}_{k''} = \sum_{\underline{i}'} \tilde{T}'_{k',\underline{i}'} (\tilde{T}'^{-1})_{\underline{i}'k''}, \tag{20}$$

where $\tilde{T}'^{-1}$ is the inverse of the matrix $\tilde{T}'$. The partition function is then expressed by

$$Z = \sum_{\underline{i},\underline{i}'} \tilde{A}_{\underline{i},\underline{i}'} M^{\tilde{A}}_{\underline{i},\underline{i}'}, \tag{21}$$

where $\tilde{A}_{\underline{i},\underline{i}'} = \sum_{k'} \tilde{T}_{k',\underline{i}} \tilde{T}'_{k',\underline{i}'}$ is defined in Eq. (9), and $M^{\tilde{A}}$ is the environment of $\tilde{A}$:

$$M^{\tilde{A}}_{\underline{i},\underline{i}'} = \sum_{k''} \left(\tilde{T}'^{-1}\right)_{\underline{i}',k''} M_{k'',\underline{i}}. \tag{22}$$

Since $\tilde{A}$ is the lower rank approximation of $A$, where $A_{\underline{i},\underline{i}'} = \sum_{\hat{k}} R_{\hat{k},\underline{i}} R'_{\hat{k},\underline{i}'}$ defined in Eq. (7), the environment $M^{\tilde{A}}$ is approximately the environment of $M^A$,

$$M^A \approx M^{\tilde{A}}. \tag{23}$$

The physical explanation of the above approximation is that, for a subsystem expressed by $\tilde{A}$ and its environment, if we replace this subsystem with another subsystem $A$, which interacts with the environment in a very similar way with more internal variable states, the environment will not change too much. From the relationship of $A$ and its environment, we get

$$Z = \sum_{\underline{i},\underline{i}',\hat{k}} R_{\hat{k},\underline{i}} R'_{\hat{k},\underline{i}'} M^A_{\underline{i},\underline{i}'}.$$

The environments of $R$ and $R'$ are obtained as

$$M^R_{\hat{k},\underline{i}} = \sum_{\underline{i}'} R'_{\hat{k},\underline{i}'} M^A_{\underline{i},\underline{i}'}, \tag{24}$$

$$M^{R'}_{\hat{k},\underline{i}'} = \sum_{\underline{i}} R_{\hat{k},\underline{i}} M^A_{\underline{i},\underline{i}'}. \tag{25}$$

We expand the grouped indices $\underline{i}$, $\underline{i}'$ of matrices $M^R$ and $M^{R'}$ and exchange the indices to get the environments $M^R_{\hat{k},j_1,\hat{i}_2,i_3}$ and $M^{R'}_{\hat{i}'_0,j'_1,\hat{k},i'_3}$ of tensors $R$ and $R'$. This is the backward iteration of the cutoff step.

The backward iteration of the contraction step is more straightforward. We unpack the indices $\hat{k}$ and $\hat{i}_2$ of $R$ in the view before contraction; hence, $R_{\hat{k},j_1,\hat{i}_2,i_3} \to R_{(i_0,j_0),j_1,(i_2,j_2),i_3} = \sum_k T_{i_0,k,i_2,i_3} T'_{j_0,j_1,j_2,k}$ as shown in Eq. (6), in which the first index $\hat{i}_0$ is the index $\hat{k}$ here. From the relation of the tensor $R$ and its environment,

$$Z = \sum_{i_0 j_0 j_1 i_2 j_2 i_3 k} T_{i_0,k,i_2,i_3} T'_{j_0,j_1,j_2,k} M^R_{(i_0,j_0),j_1,(i_2,j_2),i_3},$$

we can get the environments of $T$ and $T'$ as

$$M^T_{i_0,k,i_2,i_3} = \sum_{j_1 j_2 j_3} T'_{j_0,j_1,j_2,k} M^R_{(i_0,j_0),j_1,(i_2,j_2),i_3}, \tag{26}$$

$$M^{T'}_{j_0,j_1,j_2,k} = \sum_{i_0 i_1 i_2} T_{i_0,k,i_2,i_3} M^R_{(i_0,j_0),j_1,(i_2,j_2),i_3}. \tag{27}$$

After the above two steps, the environment matrix $M^{\hat{T}}$ is calculated by knowing the environment matrix $M$ of higher coarse-grained level tensor network. We repeat this process until the environment tensors of the original tensor network are obtained. Then the marginal probability distributions can be calculated from Eq. (16). In practice, we reduce the computational complexity by utilizing the fact that the matrix $A$ is at most rank $D^2$.

The backward iteration is initially introduced to design a better way to do tensor coarse-graining by minimizing the change of the whole system with the environments [14] on the ferromagnetic Ising model. This improvement can also be applied to the EA model in the same way. We here exploit the backward iteration to calculate local physical quantities simultaneously.

## V. NUMERICAL RESULTS

We compared the partition function calculated by our topological invariant TRG with those obtained by the original TRG [12] and mean-field approach, belief propagation and generalized belief propagation (GBP) [24,27,28], on the pure spin glass model without external fields, i.e., $p = 0.5$ and $h_i = 0$. The exact partition function is calculated by the algorithm [23]. The paramagnetic solutions of BP and GBP [27,28] is included, which is the mean-field method under the Bethe-Peierls approximation [39] and Kikuchi approximation [40], respectively. We measure the average error of the logarithm partition function as

$$\epsilon_\phi = \frac{1}{N} \langle |\ln(Z_{\text{exact}}) - \ln(Z)| \rangle \tag{28}$$

over 64 instances with $L = 64$ in Fig. 3 in the region $\beta = 1/T \in [0,1.1]$. The results show that tensor renormalization approaches outperform BP and GBP by several orders. For the same cutoff parameter $D = 8$, our topological invariant TRG is more accurate than the original TRG. If one use a larger cutoff parameter $D$, the results will be better, while the computation time will increase dramatically.

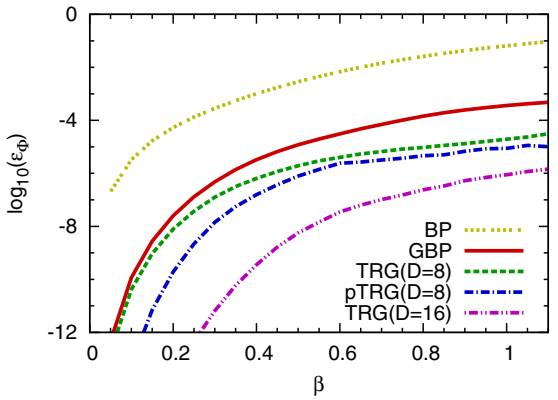


FIG. 3. (Color online) Comparison of the error of $\frac{1}{N}\ln Z$, calculated by our topological invariant TRG (pTRG) with $D = 8$, the original TRG method (TRG) [12] with $D = 8,16$, and the mean-field approaches BP and GBP [27,28]. The results are obtained by averaging over 64 instances on a periodic square lattice with side length $L = 64$.

At low temperatures $T$, i.e., high inverse temperature $\beta = 1/T$, we found that the TRG procedures may result in a negative partition function. This phenomenon happens in both the original TRG [12] and our topological invariant TRG. We tested 128 instances with the inverse temperature $\beta$ ranging from 0 to 4.0. The probability of the negative partition function is shown in Fig. 4(a) . A brief explanation is that the elements in the tensors are not constrained to be non-negative and the lower rank matrix approximation makes the final result fluctuate around the exact partition function. At low temperatures, the error is so large that the scaled partition function $Z_r$ of the finial $2 \times 2$ tensor network turned out to be compatible with a negative value. It seems like a general limitation of TRG methods applying for the models with frustrations. One could use larger cutoff parameter $D$ to reduce the probability of negative results. If one only cares about the asymptotic result for a large system, one could simply neglect the negative part, since for an infinite system the log partition function is dominated by the scaling factors $\Phi_l^{(i)}$ in each forward iteration step rather than the remaining contribution $Z_r$. To clarify this point, we define the ratio of the remaining log partition function and the leading part of the scaling factors as $r$,

$$r = \left\langle \frac{\ln |Z_r|}{\sum_l \sum_i \Phi_l^{(i)}} \right\rangle, \tag{29}$$

where $\langle\cdot\rangle$ means averaging over disorders. Numerically, we averaged 128 instances. As shown in Fig. 4, the contribution of the remaining free entropy decreases as the system size increase almost linearly in the log-log scale. For a large system, it will be even lower than the error, so that we can safely discard this term. This phenomenon also indicates that we can investigate the EA model in the thermodynamic limit, similar to the work on ferromagnetic Ising model [15]. Because of the heterogeneity, the properties of the system are captured by infinite iterations of populations of tensors rather than a single tensor iteration. We leave the analysis of infinite systems in our future work.

We plot all the nearest-pair-spin correlations of a typical single instance compared by the numerical exact values which are calculated by numerical differential of the free energy at $\beta = 1.0$. The error is defined by

$$\epsilon_c = (|\langle\sigma_i\sigma_j\rangle_{\text{pTRG}} - \langle\sigma_i\sigma_j\rangle_{\text{exact}}|). \tag{30}$$

A larger cutoff parameter $D$ will lead to better results, as shown in Fig. 5. We do not show the local magnetizations since they

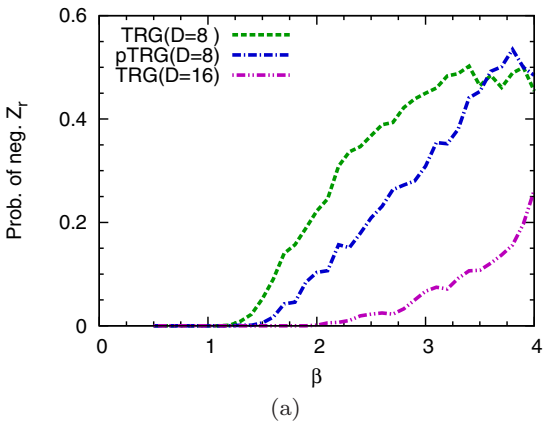


(a)

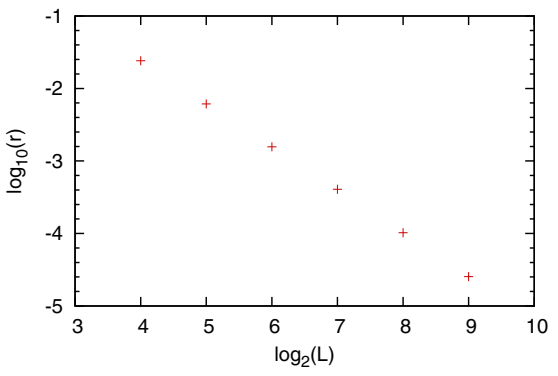


(b)

FIG. 4. (Color online) (a) The probability to obtain a negative $Z_r$ and (b) the ratio $r$ of $\ln|Z_r|$ to the leading part at $\beta = 1.5$.

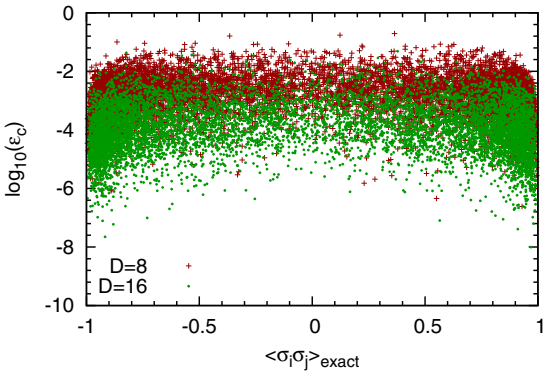


FIG. 5. (Color online) Comparing the nearest-neighbor correlations of a single instance $L = 64$ with exact results at $\beta = 1$. The cutoff parameter is set to $D = 8$ and 16.

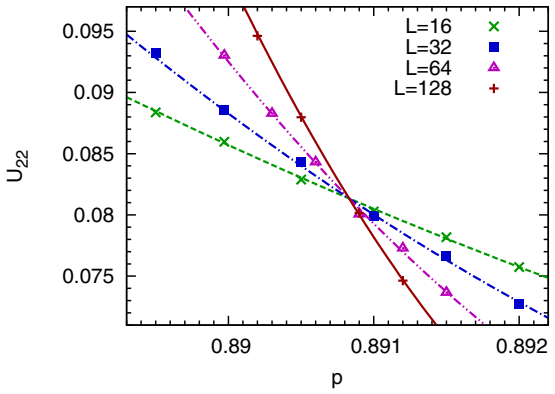


FIG. 6. (Color online) Estimation MNP point by finite size scaling. Lines are got by fitting Eq. (33).

are always zero because of the spin symmetry in the absence of no external fields.

The $p$-$T$ phase diagram of 2D EA model has been extensively investigated in the papers [29–37,41,42] and the references therein. There is no spin glass phase at finite temperature [42], while it undergoes a para-ferro-magnetic phase transition at low temperature $T$ and large $p$. The system is in the paramagnetic phase when $0.5 \leqslant p < p_c(T)$ and in the ferromagnetic phase when $p_c(T) < p \leqslant 1$. A special line $p_{\mathrm{NL}}(T) = [\tanh(1/T) + 1]/2$ is called the Nishimori line [36], on which some physical quantities can be calculated exactly. The multicritical Nishimori point (MNP) is the crossing point of the Nishimori line and the critical line $p_c(T)$. We compute the MNP by locating the crossing point.

We use the topological invariant TRG as a tool to calculate magnetizations and compute susceptibility $\chi$ by numerical differential

$$\chi = \frac{d\sum_i \langle\sigma_i\rangle}{dh}, \tag{31}$$

where $h$ is the external field and $\langle\cdot\rangle$ means averaging over the Boltzmann distribution, which can be quickly calculated by the marginal distribution Eq. (16) after the backward iteration. The MNP point is estimated by finite size scaling stated in the work [29]. We measure the RG invariant quantity $U_{22}$, along Nishimori line near MNP, where

$$U_{22} = \frac{[\chi^2]}{[\chi]^2} - 1, \tag{32}$$

where the square brackets represent the average over the disorder, i.e., the couplings $\{J_{ij}\}$. We use $2 \times 10^5$ instances for each point. Then the MNP point is got by fitting

$$U_{22} = U_{22}^* + a_1(p - p^*)L^{y_1} + a_2(p - p^*)^2 L^{2y_1}, \tag{33}$$

where $U_{22}^*$, $a_n$, $p^*$, $y_1$ are fitting parameters. We fit the data with the lattice size $16 \leqslant L \leqslant 128$ as shown in Fig. 6 and estimate the MNP point at $p^* = 0.890\,830 \pm 0.000\,22$, the exponent $y_1 = 0.642 \pm 0.022$, and other parameters $U_{22} = 0.0813 \pm 0.0003$, $a_1 = -0.85 \pm 0.07$, and $a_2 = 6.5 \pm 2.6$. The $\chi^2$ test reports a small ratio of $\chi^2$ to the degree of freedom $\chi^2/\mathrm{DOF} = 7.2/17$, which shows that the fit model is good enough to describe the data. We also test the fit by using different data groups, for example $L \geqslant 32$ and $L \leqslant 64$. All test

TABLE I. Location of the MNP.

| Methods | $p^*$ |
|---|---|
| BP [28] | 0.79 |
| GBP [27,28] | 0.85 |
| Duality analysis [32] | 0.889 972 |
| Duality analysis [33] | 0.890 813 |
| pTRG | 0.890 830(22) |
| Monte Carlo [29] | 0.890 81(7) |
| Monte Carlo [43] | 0.890 83(3) |

are consistent with each other, except the data of $L = 8$, which has strong finite size effect so that we discard it in all fits. The susceptibilities $\chi$ are checked by using different differential steps $\delta h$ ranging from $10^{-6}$ to $10^{-3}$. For most of instances, they are insensitive to $\delta h$, and we set $\delta h = 10^{-5}$. A tiny fraction (about $10^{-4}$) depends on $\delta h$, and for these cases a larger $\delta h$ is used. The location of MNP is not dependent on the choices of $\delta h$. Small portions of instances are also verified by averaging the two-point correlations. The comparison of the estimation MNP is shown in Table I. The results agree well with the recent Monte Carlo method with finite size scaling [29] and the recent duality analysis inspired by hierarchical lattice [33]. We leave the discussion of re-entrance phenomena and strong disorder universality as the future work. We emphasize that the role of TRG here is a new tool to calculate physical quantities. Compared to other methods, the mean-field estimation by BP and GBP on 2D EA model [27,28] is much better.

## VI. DISCUSSIONS AND CONCLUSION

In this paper, we applied the TRG on the 2D EA model and proposed a topological invariant tensor coarse-graining procedure, as well as an approach to calculate local physical quantities simultaneously. Two problems hidden in the translation symmetric cases are solved. We avoid overcutting the degrees-of-freedom indices in the coarse-graining procedure and avoid inversing a singular matrix in backward iterations. The backward iteration process was used to compute single spin marginal probability distributions and nearest-neighbor spin pair correlations.

We found that the TRG scheme is able to compute the free energy and local correlations accurately if the temperature is not very low. At low temperatures the TRG scheme might lead to a negative value of the partition function. We show that, for large systems, the main contribution of the partition function is the scaling factors during the coarse-graining iteration, and the negative remaining scaled partition function of the final $2 \times 2$ tensor networks can be discarded. The successful estimation of the MNP location indicates TRG can be used in studying the critical phenomena in a satisfied precision [15], though originally TRG is considered only be applied to a gapped phase [12]. The present TRG scheme cannot be applied to the case at zero temperature because the singular value decomposition (SVD) only preserves the local optimal coarse-graining mode, and they are orthogonal in the further coarse-graining iteration and finally get zero partition function. It is an open question whether TRG can be used in a zero-temperature problem. A further improvement can be made by considering the effect of

environments, which is illustrated in the paper [14,21] on the ferromagnetic Ising model. In principle, one can investigate the fixed point of TRG. However, it may not give the good precision we got in our paper, because the advantage of TRG is its excellent performance in computing physical quantities rather than analyzing the fix point of the renormalization [44].

The topic of the nature of spin glass phase on a 3D lattice is still rather active [2–7]. The main method in most of the current studies is the Monte Carlo sampling. The topological invariant coarse-graining iteration can be done in 3D cases by contracting tensors along one direction and cutting off the indices associated with the edges along the other two directions. Local physical quantities, for example, the EA parameter, can be directly gotten, as shown in this paper. The sample-to-sample overlap distribution or other nonlocal quantities would be estimated by TRG guided sampling, in the way that we fix the spins one by one according to its marginal probability. So, it presents an alternative way to investigate 3D spin glass models.

Another application is in investigating combinatorial optimization problems on finite-dimensional lattices or loopy random graphs. TRG can be immediately applied on image segmentation and denoising [8]. They share the same mathematical structure as the 2D spin glass model. For the random graph model, the mean-field method provided excellent solutions on mean-field-like systems, such as the local-tree-like structured graph [45] and fully connected graph [46]. For the system rich in local loops, the mean-field approximation may not be quite accurate, for example, small world networks and many real networks. The extension of TRG on a general graph provides a new insight and maybe another physics-based solution to such problems. Similar to the belief propagation, the decimation [47] and reinforcement approaches [48] can be combined with TRG to get optimization solutions.

## ACKNOWLEDGMENTS

We thank Qiao-Ni Chen, Zhi-Yuan Xie, Jin-Fang Fan, Jack Raymond, and Victor Martin-Mayor for helpful discussions and Jack Raymond for comments on an earlier version of the manuscript. H.-J.Z. was supported by the National Basic Research Program of China (Grant No. 2013CB932804), the Knowledge Innovation Program of Chinese Academy of Sciences (Grant No. KJCX2-EW-J02), and the National Science Foundation of China (NSFC) (Grants No. 11121403 and No. 11225526). The numerical simulations were performed in the HPC computer cluster of ITP-CAS and we thank Dr. Hongbo Jin for technical help.

## APPENDIX: SIMPLIFYING SINGULAR VALUE DECOMPOSITION OF MATRIX *A*

We started from the definition of the matrix $A$ in Eq. (7), where $R$ and $R'$ are tensors with four indices. The simplifying cutoff step is graphically showed in Fig. 7. We exchange

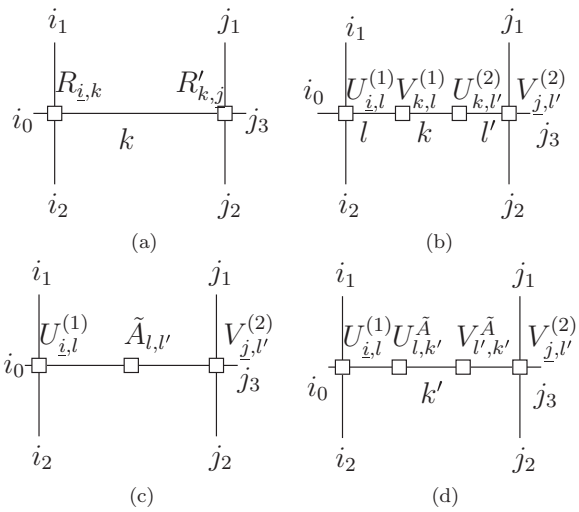


FIG. 7. Demonstration of simplifying cutoff step.

and combine the indices so that $R_{\hat{k},j_1,\hat{i}_2,i_3}$, $R'_{\hat{i}'_0,j'_1,\hat{k},i'_3}$ change to matrices $\hat{R}_{(j_1,\hat{i}_2,i_3);\hat{k}}$, $\hat{R}'_{(\hat{i}'_0,j'_1,i'_3);\hat{k}}$. For simplicity, we write $\underline{i}=(j_1,\hat{i}_2,i_3)$ and $\underline{i}'=(\hat{i}'_0,j'_1,i'_3)$. Instead of multiplying $R$ and $R'$, here we first decompose them by the singular value decomposition

$$R_{\underline{i},k}=\sum_l U_{\underline{i},l}d_l V_{l,k}, \tag{A1}$$

$$R'_{k,\underline{i}'}=\sum_{l'} U'_{k,l'}d_l V'_{l',\underline{i}'}. \tag{A2}$$

Let

$$\tilde{A}_{l,l'}=\sum_k d_l V_{l,k}U'_{k,l'}d_l. \tag{A3}$$

We decompose $\tilde{A}$ by the singular value decomposition

$$\tilde{A}_{l,l'}=\sum_{k'} U^A_{l,k'}d^A_{k'}V^A_{l',k'}. \tag{A4}$$

Then tensors $\tilde{T}_{\underline{i},k'},\tilde{T}'_{\underline{j},k'}$ in Eq. (9) could be calculated by

$$\tilde{T}_{\underline{i},k'}=\sum_l U_{\underline{i},l}U^A_{l,k'}d_l^{A\frac{1}{2}}, \tag{A5}$$

$$\tilde{T}'_{\underline{i}',k'}=\sum_{l'} d_l^{A\frac{1}{2}}V^A_{l',k'}V'_{l',\underline{i}'}. \tag{A6}$$

The numerical SVD routines take $O(mn^2)$ flops to decompose a $m\times n$ matrix ($m\geqslant n$) by Golub-Reinsch algorithm [49]. The SVD routine in the GNU Scientific Library is used in our numerical calculation. The maximum size of matrix $\hat{R}$, and $\hat{R}'$ are $D^4\times D$. The SVD of these two matrices takes $O(D^8)$ flops, which take most computational complexity in the coarse-graining step, while directly decomposing the $D^6\times D^6$ matrix $A$ in Eq. (8) takes $O(D^{18})$ flops.

[1] S. F. Edwards and P. W. Anderson, J. Phys. F: Met. Phys. **5**, 965 (1975).
[2] G. Parisi, Phys. Rev. Lett. **50**, 1946 (1983).
[3] D. S. Fisher and D. A. Huse, Phys. Rev. B **38**, 386 (1988).
[4] B. Yucesoy, H. G. Katzgraber, and J. Machta, Phys. Rev. Lett. **109**, 177204 (2012).

[5] A. Billoire, L. A. Fernandez, A. Maiorano, E. Marinari, V. Martin-Mayor, G. Parisi, F. Ricci-Tersenghi, J. J. Ruiz-Lorenzo, and D. Yllanes, Phys. Rev. Lett. **110**, 219701 (2013).

[6] C. K. Thomas, D. A. Huse, and A. A. Middleton, Phys. Rev. Lett. **107**, 047203 (2011).

[7] F. Parisen Toldin, A. Pelissetto, and E. Vicari, Phys. Rev. E **84**, 051116 (2011).

[8] K. Tanaka, J.-i. Inoue, and D. Titterington, J. Phys. A **36**, 11023 (2003).

[9] H. Derin and H. Elliott, IEEE Trans. Pattern Anal. Mach. Intell. **9**, 39 (1987).

[10] J. Sun, N.-N. Zheng, and H.-Y. Shum, IEEE Trans. Pattern Anal. Mach. Intell. **25**, 787 (2003).

[11] S. Z. Li, in *Computer Vision ECCV'94* (Springer, Berlin, 1994), pp. 361–370.

[12] M. Levin and C. P. Nave, Phys. Rev. Lett. **99**, 120601 (2007).

[13] U. Schollwöck, Rev. Mod. Phys. **77**, 259 (2005).

[14] Z.-Y. Xie, H.-C. Jiang, Q.-N. Chen, Z.-Y. Weng, and T. Xiang, Phys. Rev. Lett. **103**, 160601 (2009).

[15] M. Hinczewski and A. N. Berker, Phys. Rev. E **77**, 011104 (2008).

[16] C. Güven, M. Hinczewski, and A. N. Berker, Phys. Rev. E **82**, 051110 (2010).

[17] C. Güven and M. Hinczewski, Phys. A **389**, 2915 (2010).

[18] H.-C. Jiang, Z.-Y. Weng, and T. Xiang, Phys. Rev. Lett. **101**, 090603 (2008).

[19] Z.-C. Gu, M. Levin, and X.-G. Wen, Phys. Rev. B **78**, 205116 (2008).

[20] W. Li, S.-J. Ran, S.-S. Gong, Y. Zhao, B. Xi, F. Ye, and G. Su, Phys. Rev. Lett. **106**, 127202 (2011).

[21] Z.-Y. Xie, J. Chen, M.-P. Qin, J.-W. Zhu, L.-P. Yang, and T. Xiang, Phys. Rev. B **86**, 045139 (2012).

[22] A. García-Sáez and J. I. Latorre, Phys. Rev. B **87**, 085130 (2013).

[23] F. Barahona, J. Phys. A **15**, 3241 (1982).

[24] J. S. Yedidia, W. T. Freeman, and Y. Weiss, IEEE Trans. Inf. Theory **51**, 2282 (2005).

[25] H.-J. Zhou, C. Wang, J.-Q. Xiao, and Z.-D. Bi, J. Stat. Mech.: Theor. Exp. (2011) L12001.

[26] H.-J. Zhou and C. Wang, J. Stat. Phys. **148**, 513 (2012).

[27] C. Wang and H.-J. Zhou, J. Phys.: Conf. Ser. **473**, 012004 (2013).

[28] A. Lage-Castellanos, R. Mulet, F. Ricci-Tersenghi, and T. Rizzo, J. Phys. A **46**, 135001 (2013).

[29] M. Hasenbusch, F. Parisen Toldin, A. Pelissetto, and E. Vicari, Phys. Rev. E **77**, 051115 (2008).

[30] Y. Ozeki and H. Nishimori, J. Phys. Soc. Jpn. **56**, 3265 (1987).

[31] C. K. Thomas and A. A. Middleton, Phys. Rev. E **87**, 043303 (2013).

[32] H. Nishimori and K. Nemoto, J. Phys. Soc. Jpn. **71**, 1198 (2002).

[33] M. Ohzeki, Phys. Rev. E **79**, 021129 (2009).

[34] M. Ohzeki, C. K. Thomas, H. G. Katzgraber, H. Bombin, and M. Martin-Delgado, J. Stat. Mech.: Theor. Exp. (2011) P02004.

[35] T. Jörg and F. Krzakala, J. Stat. Mech.: Theor. Exp. (2012) L01001.

[36] H. Nishimori, Prog. Theor. Phys. **66**, 1169 (1981).

[37] K. Takeda, T. Sasamoto, and H. Nishimori, J. Phys. A **38**, 3751 (2005).

[38] P. W. Kasteleyn, Physica **27**, 1209 (1961).

[39] H. A. Bethe, Proc. R. Soc. London. Ser. A **150**, 552 (1935).

[40] R. Kikuchi, Phys. Rev. **81**, 988 (1951).

[41] F. D. Nobre, Phys. Rev. E **64**, 046108 (2001).

[42] R. N. Bhatt and A. P. Young, Phys. Rev. B **37**, 5606 (1988).

[43] F. Parisen Toldin, A. Pelissetto, and E. Vicari, J. Stat. Phys. **135**, 1039 (2009).

[44] E. Efrati, Z. Wang, A. Kolan, and L. P. Kadanoff, Rev. Mod. Phys. **86**, 647 (2014).

[45] M. Mézard and G. Parisi, Eur. Phys. J. B **20**, 217 (2001).

[46] D. Sherrington and S. Kirkpatrick, Phys. Rev. Lett. **35**, 1792 (1975).

[47] M. Mézard and R. Zecchina, Phys. Rev. E **66**, 056126 (2002).

[48] J. Chavas, C. Furtlehner, M. Mézard, and R. Zecchina, J. Stat. Mech.: Theor. Exp. (2005) P11016.

[49] G. H. Golub and C. Reinsch, Numerische Math. **14**, 403 (1970).